ADVANCED OPTICAL MATERIALS
www.advopticalmat.de

Large Gain, Low Noise Nanocomposite Ultraviolet Photodetectors with a Linear Dynamic Range of 120 dB

*Yanjun Fang, Fawen Guo, Zhengguo Xiao, and Jinsong Huang**

The quick progress in organic photovoltaic research and development gives rise to a new application of organic electronic devices in weak-light sensing. In addition to the inherent advantages of organic electronic devices, such as being low cost, flexible and lightweight,[1] organic photodetectors can be made potentially with superior performance to the inorganic counterpart due to some unique properties of organic semiconductor materials.[2] The dark current of organic diodes can be very low due to the low un-intentional doping density in intrinsic organic semiconductors. Spray-coated organic photodetectors based on bulk-heterojunction structures have been demonstrated to have comparable performance with those of the best inorganic counterparts, such as silicon photodiodes.[1b,3]

Since the detectivity of a photodetector is determined by the signal-to-noise ratio, recent discovery of high gain in fullerene-based (C_{60}) organic diode devices added the promise of organic photodetectors as potential candidates to replace inorganic counterparts.[4] It was demonstrated by us that a high gain above 50 from a C_{60} device with a structure of indium tin oxide (ITO)/poly(3,4-ethylenedioxythiophene):poly(styrenesulfonate) (PEDOT:PSS) (35 nm)/C_{60} (80 nm)/2,9-dimethyl-4,7-diphenyl-1,10-phenanthroline (BCP) (20 nm)/Al (100 nm) could be achieved under relatively low reverse bias of –4 V. The high gain was proposed to be caused by an interfacial trap-controlled charge injection mechanism.[4a] The trapped holes in the C_{60} close to PEDOT:PSS, excited by incident photons, reduce the energy barrier between the Fermi energy of PEDOT:PSS and LUMO of C_{60}, and induced strong secondary electron injection under reverse bias.[4a] However, despite the large gain, the specific detectivity of such fullerene photodetectors was not high compared to inorganic UV photodetectors because of their relatively large dark current. The disorder of n-type C_{60} causes the hole traps in it, which is the origin of the high gain, however brings in a relatively strong electron injection with a dark current density of about 1 mA/cm^2 under reverse bias of –8 V.[4b] To address this issue, we recently introduced a cross-linkable buffer layer, 4,4′-Bis[(p-trichlorosilylpropylphenyl) phenylamino]-biphenyl (C-TPD), at the interface of PEDOT:PSS and C_{60} to reduce the dark current. The pin-hole free and conformal C-TPD buffer layer dramatically reduced the dark current density by 3–4 orders of magnitude. The significantly reduced dark current enabled a constant responsivity from light intensity of 10^{-2} Wcm^{-2} all the way down to 12 pWcm^{-2}, resulting in a very large linear dynamic range of 90 dB.[5] However, the insertion of 25 nm C-TPD between PEDOT:PSS and C_{60} interface also blocked the tunneling of electrons (secondary electron injection) into C_{60} even under large reverse bias of –6 V, and thus annulled the gain of C_{60} photodetectors.

In this manuscript, we report on a fullerene based photodetector with both large gain and low noise, enabled by the introduced C-TPD:ZnO nanocomposite buffer layer between the PEDOT:PSS and C_{60} layer. As a result, a record large linear dynamic range of 120 dB was achieved in these organic photodetectors which almost doubles that of the state-of-the-art commercial inorganic UV solid-state photodetectors.

The device structure used here is shown in **Figure 1**(a), which is composed of ITO (cathode)/PEDOT:PSS (35 nm)/C-TPD:ZnO (weight ratio 1:1) (30 nm)/C_{60} (80 nm)/BCP (10 nm)/Al (anode) (100 nm). The C-TPD was formed via a thermal annealing assisted hydrolysis process of TPD-Si_2, and its chemical structure is shown in Figure 1(b). C_{60} was chosen as the photoactive material for its demonstrated high photoconductive gain and strong absorption in the ultraviolet–blue range.[4a] Compared to our previously reported device,[5] ZnO nanoparticles were introduced into the C-TPD layer here. ZnO is a wide band gap semiconductor material, and also a potential alternative to GaN as the UV absorption material due to its merits of low cost and easy fabrication.[6] The morphology of the C-TPD:ZnO layer was characterized by atomic force microscope (AFM), which is shown in Figure 1(c). The surface roughness of C-TPD:ZnO layer is 2.1 nm, which is higher than the C-TPD layer of 0.41 nm.[5] From the UV–vis absorption spectra shown in Figure 1(d), ZnO nanoparticles shows strong light absorption in the UV range, while the C_{60} layer's absorption spectrum covers a wide range from UV to blue–green region. As a result, the absorption of the device covers the UV–visible range. Besides the strong UV absorption capacity, ZnO nanoparticles also possess large quantities of traps on the surface due to the large surface-to-volume ratio and hence high concentration of surface states.[6] In our previous study, we have demonstrated a ZnO/polymer hybrid UV photodetector with an extremely high gain of 4000, which is based on the interfacial trap-controlled charge injection mechanism.[7] Inspired by that, it is expected that the ZnO nanoparticles in the C-TPD layer of the C_{60} photodetector may also behave as a photon-switchable valve to control the electron injection, and thus can recover its original high photoconductive gain.

The device performance was firstly characterized by the external quantum efficiency (EQE) measurements. The measured EQE curves under different applied reverse biases are shown in **Figure 2**(a). The EQE values continuously increase

Dr. Y. Fang, Dr. F. Guo, Z. Xiao, Prof. J. Huang
Department of Mechanical and Materials Engineering
Department of Electrical Engineering
and Nebraska Center for Materials and Nanoscience
University of Nebraska-Lincoln
Lincoln, Nebraska 68588–0656, USA
E-mail: jhuang2@unl.edu

DOI: 10.1002/adom.201300530

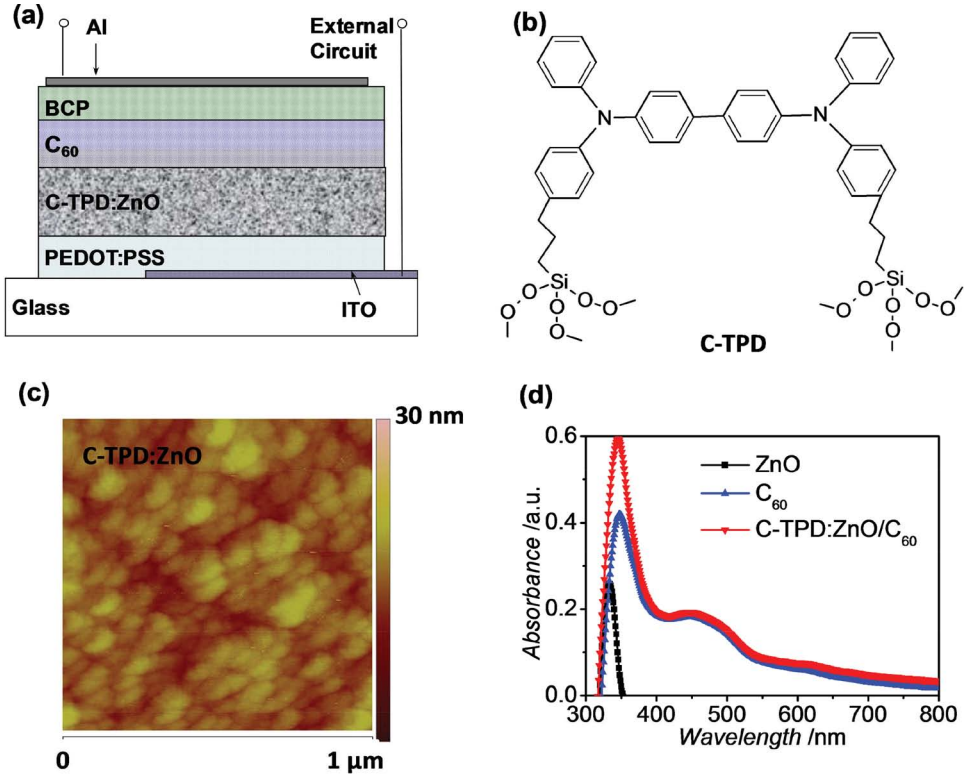

Figure 1. (a) Schematic layout of the device structure (not to scale). (b) The chemical structure of C-TPD. (c) The AFM image of the C-TPD:ZnO layer. (d) The UV–vis absorption spectra of ZnO nanoparticle layer, C_{60} layer, and C-TPD:ZnO/C_{60} double layer.

throughout the UV-vis spectrum with the increase of the reverse bias. The peak values exceed 100% when the reverse bias is above –6 V, and further increase to 408% at 390 nm under the reverse bias of –8 V. The corresponding responsivity R_{es} can be calculated from EQE by:

$$R_{es} = \frac{EQE}{hv} \quad (1)$$

where hv is the energy of the incident photon in electronvolts. The peak responsivity is calculated to be 1.28 A/W at 390 nm, which is more than five times larger than those of commercial SiC and GaN UV detector (less than 0.2 A/W).[7] This EQE value is also over one order of magnitude higher than the device without the addition of ZnO nanoparticles in the C-TPD layer, which indicates the role of ZnO nanoparticles in inducing high gain in the device. The dark current and photocurrent traces of the device are shown in Figure 2(b). It is found that the dark current is comparable to our previous device without ZnO nanoparticles, but a transition from a photodiode to a photoconductor occurs under illumination with the light intensity of 0.1 Wcm^{-2}, which leads to a large photocurrent. This means that the introduction of ZnO nanoparticles into the C-TPD buffer layer induces a large gain while does not compromise

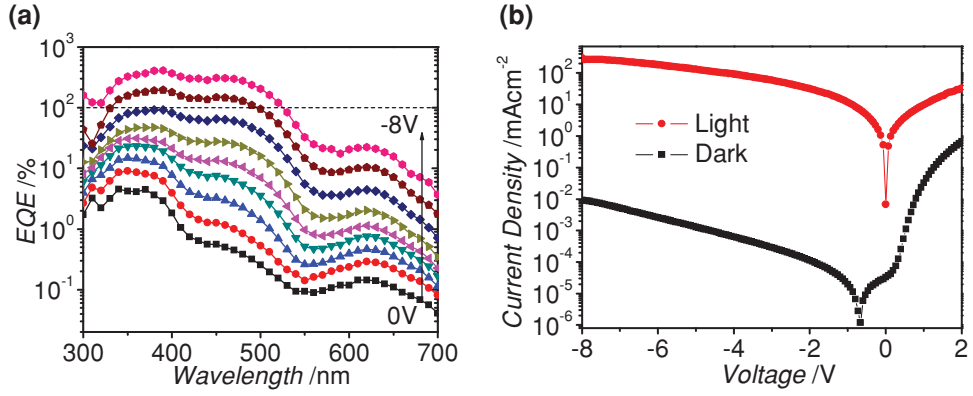

Figure 2. (a) EQEs of the photodetector under the reverse bias from 0 V to –8 V with a voltage step of 1 V. (b) Photocurrent density at light intensity of 0.1 Wcm^{-2} and dark current density of the device.

Adv. Optical Mater. 2014,
DOI: 10.1002/adom.201300530

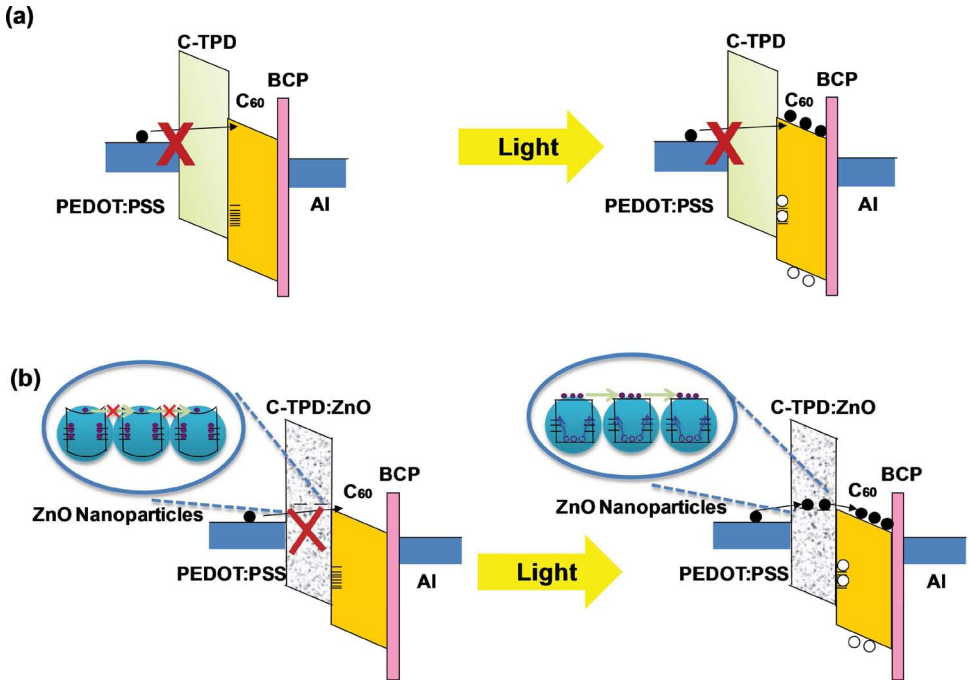

Figure 3. Energy band diagrams of the reverse-biased photodetectors in the dark and under the illumination: (a) without and (b) with ZnO nanoparticles in the C-TPD buffer layer.

the low dark current of the detector, which is very beneficial to its light detection performance.

The working principle of the photodetector can be understood by the energy band diagrams shown in **Figure 3**. It is shown that under reverse bias, when no ZnO nanoparticles are added into the C-TPD layer (Figure 3(a)), the electron injection from PEDOT:PSS to C_{60} is blocked by the C-TPD layer owing to its low electron mobility and the large electron injection barrier of about 2.8 eV. Therefore, the hole trap induced electron injection at the PEDOT:PSS/C_{60} interface is largely hampered under illumination, which results in the loss of gain of the device. For the device with C-TPD:ZnO nanocomposite as the buffer layer (Figure 3(b)), although ZnO is a good electron transport material, the large amount of surface states on the ZnO nanoparticles will induce the upward bending of the energy band.[6b] It leads to the formation of low-conductivity depletion layer on the surface, and hence the energy barrier between nanoparticles that obstructs the transportation of electrons through the buffer layer.[6] Therefore, the low dark current can still be maintained. In contrast, when light is illuminated onto the device, both the ZnO nanoparticles and C_{60} layer will absorb the incident light and generate excitons. The photo generated electrons and holes will move towards opposite directions under the applied reverse bias, with the electrons running towards the anode while the holes flowing to the C-TPD:ZnO layer. Due to the large quantities of hole-traps on the surface of ZnO nanoparticles, the photon-generated holes tend to be trapped by the ZnO nanoparticles instead of being collected by the cathode. The trapped holes then recombine with the electrons on the surface states, therefore alleviate the energy bending near the surface and reduce the width of the depletion layer.[6] As a result, electrons can readily transport between ZnO nanoparticles with a small reverse bias. In this way, the electron transport between PEDOT:PSS and C_{60} is no longer blocked under illumination, thus the interfacial hole trap induced electron injection at the C_{60} layer is recovered, which leads to a high gain and large photocurrent.

In order to verify the role played by the C-TPD:ZnO layer in the photodetector, the electron-only and hole-only devices were fabricated with the C-TPD:ZnO composite as the carrier transport layer. The corresponding J-V curves (Figure S1(a)) exhibit that the electron current density is three to four orders of magnitude lower than the hole current density. This means that the C-TPD:ZnO layer is not a good electron transport material in the dark, so it can function as an electron blocking layer to reduce the dark current of the detector, just like the C-TPD layer. To further confirm the electron conductivity of the device under illumination, electron-only device was fabricated by replacing the PEDOT:PSS with Cs_2CO_3 in the original photodetector device. It is found that under the light illumination, the current density under reverse bias increases by three orders of magnitude, which demonstrates that the device changes to electron conductor under illumination (Figure S1(b)).

In order to identify the origin of the traps in the devices, the capacitance versus frequency measurement of the photodetector was performed in the dark as well as under the illumination of UV or green light. During the sweeping of the frequency from high to low values, the demarcation energy is moved from below the Fermi-level, where no states can respond, to above the trap levels, where all states respond.[8] In this way, we can obtain the trap distribution in the active layers. It is shown in **Figure 4**(a) that under the illumination of green light, as the frequency is swept from high to low values, there is an evident inflection point at around 10^2 Hz; when the device is

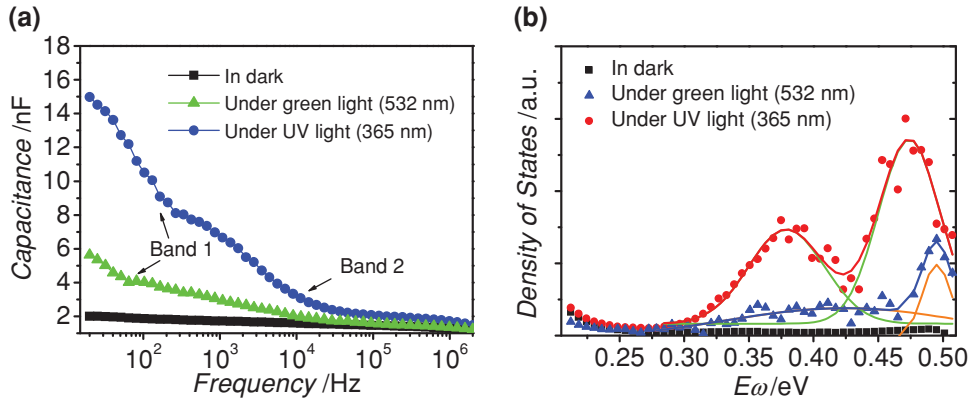

Figure 4. (a) The capacitance versus frequency curves of the device measured in the dark and under the illumination of UV or green light with light intensity of 30 mWcm^{-2}. (b) The calculated trap density of states versus demarcation energy curves of the device fitted by the Gaussian distribution.

illuminated under UV light, besides the inflection point at low frequency, there is an additional one at around 10^4 Hz. Since ZnO only has UV response while C_{60} can respond to both UV and green light based on the absorption spectrum, we can speculate that the inflection point at high frequency corresponds to the trap band from the ZnO layer, while the one at low frequency is related to the trap band in C_{60} layer. The distribution of the trap bands can be more straightforwardly presented by the calculated trap density of states verses demarcation energy curves of the device (Figure 4(b)) following the route proposed by Carr et al.[8,9] The demarcation energy E_ω correlates with the applied frequency by the following expression:

$$E_\omega = k_B T Ln \frac{\omega_0}{\omega} \tag{2}$$

where ω_0 is the attempt-to-escape frequency, ω is the applied angular frequency, k_B is the Boltzmann constant, and T is the absolute temperature. For reference, an attempt-to-escape frequency of 5×10^{10} s^{-1} was used here. And the distribution of trap density of states N_T can be calculated by:

$$N_T(E_\omega) = -\frac{V_{bi}}{Wq}\frac{dC}{d\omega}\frac{\omega}{k_B T} \tag{3}$$

where V_{bi} is the build-in potential, W is the width of the depletion region, and q is the elementary charge. After fitting the curves with the Gaussian distribution, it is seen that there are two kinds of trap bands existing in the device. For the same reason mentioned above, the deeper trap band can be attributed to the traps in the C_{60} layer, while the shallower trap band comes from the ZnO nanoparticles. The result further proves that ZnO nanoparticles bring in additional traps in the device, which can behave as the photo-switchable valve to control the electron injection.

Since the device possesses high gain and low dark current simultaneously, it is expected to have high detectivity and should be very potential in weak light detection. The figure of merit to characterize the capability of weak light detection for a photodetector is the noise equivalent power (NEP), which is given by:[10]

$$NEP = \frac{i_n^{2-1/2}}{R_{es}} \tag{4}$$

where $i_n^{2-1/2}$ is the noise current. In order to obtain the NEP value of our photodetector, the noise current was measured by using a Stanford Research SR830 Lock-In amplifier following the route reported previously.[11] During the measurement, the lock-in frequency of the noise current was set to be 35 Hz, so that it was consistent with the frequency used in EQE measurement. The measured noise current is shown in **Figure 5**(a). The thermal noise limit is also shown in the figure for comparison, which is calculated by $i_{n,th} = \sqrt{4k_B TB/R}$, where B is the bandwidth, and R is the resistance of the detector. It can be seen that the noise current is extremely small and even close to the thermal

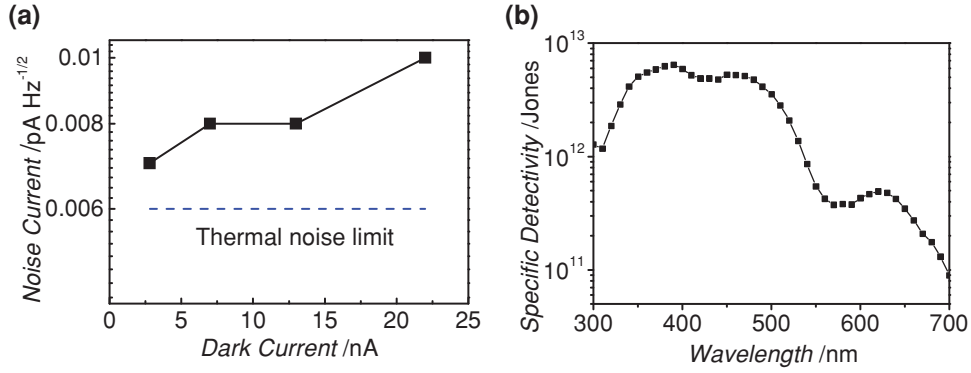

Figure 5. (a) The measured noise current under different reverse bias voltages, and (b) the calculated specific detectivity of the photodetector at –6 V.

Adv. Optical Mater. 2014,
DOI: 10.1002/adom.201300530

noise limit under low reverse bias. The noise current at –6 V is only 0.01 pAHz$^{-1/2}$, which is more than one order of magnitude lower than our previous device with C-TPD as the buffer layer. It is not clear yet why the introduction of ZnO into the buffer layer can significantly reduce the noise. Konstantatos et al.[11] have performed the noise current study of PbS quantum dot photodetectors with different surface oxidation degree and thus different kinds of trap states, and found that the neck-then-oxidize nanoparticle devices exhibited nearly five times lower noise current than that of the oxidize-then-neck devices. Hence, we infer that the reduced noise current in our case might also be related to the different carrier trap states in ZnO nanoparticles and in the C-TPD layer that result in different noise current levels during the carrier transportation. However, detailed noise power density spectrum study is needed in the future to explore the origin behind it. Due to the high responsivity and low noise current, the calculated NEP of the device is only about 34 fWHz$^{-1/2}$, which shows its bright prospect in weak light detection. The specific detectivity (D*) is a typical figure of merit used to compare the performance of different photodetectors, which is given by:[10]

$$D^* = \frac{\sqrt{AB}}{i_n/R_{es}} \quad (5)$$

where A is the effective device area, B is the bandwidth. Thanks to the high gain and low noise current, the peak specific detectivity of the device reaches 6.5×10^{12} Jones at 390 nm with the reverse bias of –6 V as shown in Figure 5(b), which is more than one order of magnitude larger than the device without the addition of ZnO nanoparticles in the buffer layer. This value also approaches that of the commercial GaN UV detector (about 2×10^{13} Jones).[7]

In the above calculation, the responsivity is obtained based on the EQE value measured at relatively high light intensity (1 μWcm^{-2}). However, the responsivity may decrease with the decrease of the light intensity due to the influence of the traps.[7] So the low NEP calculated on the basis of the responsivity measured at high light intensity does not necessarily mean its high light detection ability for very weak light near NEP. One typical example is that our previously reported nanocomposite photodetector lost its linearity at weak light intensity.[7] One of the possible reason is that ZnO nanoparticles far away from the interface do not cause useful band bending for secondary charge injection. Pushing ZnO toward the interface valve in this work should allow the very weak light to turn on the interfacial valve, and thus allow a more sensitive detection under weak light. Therefore, the linear dynamic range (LDR) of the device, which characterizes the light intensity range where the responsivity of the device keeps constant, needs to be measured to identify if the responsivity is independent of the incident light power density. The LDR was measured by recording the photocurrent at –8 V, with varied light intensities from 0.1 Wcm^{-2} all the way down to around 10^{-13} Wcm^{-2}, and the corresponding result is shown in **Figure 6**. It is seen that the device exhibits a linear photoresponse within the whole light intensity range used here, thus yielding a linear dynamic range of 120 dB. This value is 30 dB larger than the previous C_{60} detector with C-TPD as the buffer layer. This is because the device possesses much lower NEP, and at the same time does not show photocurrent saturation under illumination of high light intensity. The 120 dB LDR is significantly larger than those of the InGaAs detector[1c] (66 dB) and GaN detector[12] (50 dB), better than that of the polymer photodetector[1c] (100 dB), and even on par with that of the Si photodetector[1c] (120 dB). In fact, the 120 dB LDR is among the highest up-to-date LDR values for both inorganic and organic photodetectors.[1c,13] Such good linear response of the device over a wide light intensity range is believed to be contributed by the excellent free electron generation, transportation capabilities and low electron traps of fullerene that decrease the charge recombination probability,[5] as well as the high light absorbance and low noise current of ZnO nanoparticles that extends the upper and lower limits of the light response range.

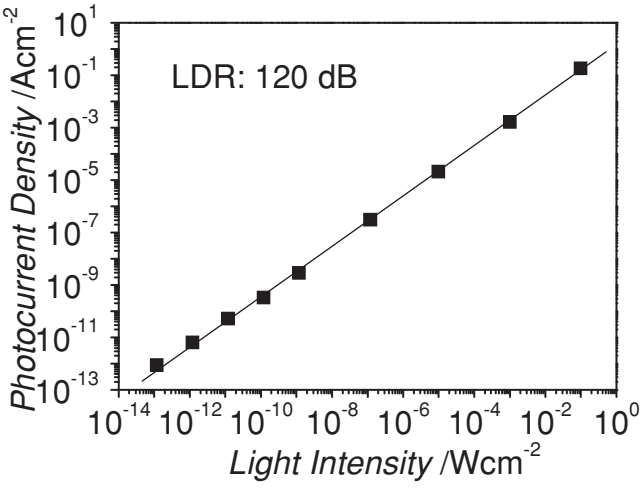

Figure 6. The dynamic response of the photodetector measured with bias of –8 V.

In summary, the ZnO nanoparticles have been introduced into the C-TPD buffer layer of the fullerene-based photodetector to successfully increase the photoconductive gain and reduce the noise current. The peak EQE value of around 400% and the peak specific detectivity of 6.5×10^{12} Jones at the wavelength of 390 nm, along with the record high LDR of 120 dB, enable the photodetector to be used in wide range of applications such as imaging, communication, and defense. The extremely high sensitivity of the photodetector also makes it particularly attractive for very weak light detection.

Experimental Section

C_{60} was purchased from Nano-C; BCP was purchased from SIGMA-ALDRICH; PEDOT:PSS was purchased from H.C.STARCK; All materials were used as received without any purification. TPD-Si_2 was synthesized following the route from literature.[14] ZnO nanoparticles were prepared using a hydrolysis method in methanol with some modifications.[7] The device is fabricated by first spin-coating PEDOT:PSS onto a clean ITO glass substrate at a spin speed of 3000 rpm, and then baked at 120 °C for 30 min. Then a ZnO nanoparticles and TPD-Si_2 hybrid solution with the weight ratio of 1:1 was spin-coated onto the PEDOT:PSS layer and baked at 100 °C in the air for 60 min to get it cross-linked. After that, C_{60}, BCP and Al were sequentially evaporated onto the C-TPD:ZnO layer with the thickness of 80 nm, 10 nm, and 100 nm, respectively.

The topography of the C-TPD:ZnO layer was characterized by atomic force microscope (AFM, Multimode Nanoscope IIIA, Veeco Metrology

Inc.) in the tapping mode. The UV-vis absorption spectra of the samples were measured by an Evolution 201 Spectrophotometer. The EQE was measured by a Newport Quantum Efficiency measurement kit with the incident monochromatic light to be modulated at the frequency of 35 Hz and the optical power density to be controlled at around 1 μWcm^{-2}. The capacitance verses frequency measurement was performed on an E4980A Precision LCR Meter, and the illumination of UV and green lights during the measurement were provided by a 365 nm laser diode and a 532 nm laser diode, respectively, with the light intensity of 30 $mWcm^{-2}$. For the dynamic range measurement, different light sources with various light intensities were used. For the light intensity below 1 μWcm^{-2}, the monochromatic illumination was provided by a 350 nm LED with a function generator to supply the modulated bias. For higher light intensity up to 0.1 Wcm^{-2}, Xe lamp was used. The UV part of the light from Xe lamp is calculated by the integration of UV light intensity from Xe lamp spectrum. The irradiance was first calibrated by a Si photodiode at the highest light intensity of each light source, and then attenuated by Newport neutral density filters.

Supporting Information

Supporting Information is available from the Wiley Online Library or from the author.

Acknowledgements

Y. Fang and F. Guo contributed to this work equally. This work is supported by Office of Naval Research (ONR, grant no. N000141210556) and US Defense Threat Reduction Agency (DTRA, award number HDTRA1–10–1–0098).

Received: December 20, 2013
Revised: February 3, 2014
Published online:

[1] a) P. Peumans, V. Bulović, S. R. Forrest, *Appl. Phys. Lett.* **2000**, *76*, 3855; b) T. Rauch, M. Boberl, S. F. Tedde, J. Furst, M. V. Kovalenko, G. Hesser, U. Lemmer, W. Heiss, O. Hayden, *Nat. Photon.* **2009**, *3*, 332; c) X. Gong, M. Tong, Y. Xia, W. Cai, J. S. Moon, Y. Cao, G. Yu, C.-L. Shieh, B. Nilsson, A. J. Heeger, *Science* **2009**, *325*, 1665.
[2] a) F.-C. Chen, S.-C. Chien, G.-L. Cious, *Appl. Phys. Lett.* **2010**, *97*, 103301; b) S.-T. Chuang, S.-C. Chien, F.-C. Chen, *Appl. Phys. Lett.* **2012**, *100*, 013309; c) L. Li, F. Zhang, Q. An, Z. Wang, J. Wang, A. Tang, H. Peng, Z. Xu, Y. Wang, *Opt. Lett.* **2013**, *38*, 3823.
[3] a) S. F. Tedde, J. Kern, T. Sterzl, J. Furst, P. Lugli, O. Hayden, *Nano Lett.* **2009**, *9*, 980; b) M. Binda, D. Natali, A. Iacchetti, M. Sampietro, *Adv. Mater.* **2013**, *25*, 4335.
[4] a) J. Huang, Y. Yang, *Appl. Phys. Lett.* **2007**, *91*, 203505; b) J. Reynaert, V. I. Arkhipov, P. Heremans, J. Poortmans, *Adv. Funct. Mater.* **2006**, *16*, 784.
[5] F. Guo, Z. Xiao, J. Huang, *Adv. Opt. Mater.* **2013**, *1*, 289.
[6] a) Y. Jin, J. Wang, B. Sun, J. C. Blakesley, N. C. Greenham, *Nano Lett.* **2008**, *8*, 1649; b) C. Soci, A. Zhang, B. Xiang, S. A. Dayeh, D. P. R. Aplin, J. Park, X. Y. Bao, Y. H. Lo, D. Wang, *Nano Lett.* **2007**, *7*, 1003.
[7] F. W. Guo, B. Yang, Y. B. Yuan, Z. G. Xiao, Q. F. Dong, Y. Bi, J. S. Huang, *Nat. Nanotechnol.* **2012**, *7*, 798.
[8] J. A. Carr, S. Chaudhary, *Energy Environ. Sci.* **2013**, *6*, 3414.
[9] J. A. Carr, S. Chaudhary, *J. Appl. Phys.* **2013**, *114*, 064509.
[10] *Photonic Devices* (Ed: J.-M. Liu), Cambridge University Press, UK **2005**.
[11] G. Konstantatos, I. Howard, A. Fischer, S. Hoogland, J. Clifford, E. Klem, L. Levina, E. H. Sargent, *Nature* **2006**, *442*, 180.
[12] M. A. Khan, J. N. Kuznia, D. T. Olson, J. M. Van Hove, M. Blasingame, L. F. Reitz, *Appl. Phys. Lett.* **1992**, *60*, 2917.
[13] a) X. L. Liu, H. X. Wang, T. B. Yang, W. Zhang, X. Gong, *Acs. Appl. Mater. Inter.* **2012**, *4*, 3701; b) G. Konstantatos, J. Clifford, L. Levina, E. H. Sargent, *Nat. Photon.* **2007**, *1*, 531.
[14] Q. Huang, J. Li, T. J. Marks, G. A. Evmenenko, P. Dutta, *J. Appl. Phys.* **2007**, *101*, 093101.